Bimeron Traveling on the Magnetic Domain Wall

Jiwen Chen,[1] Laichuan Shen,[2] Hongyu An,[3] Hua Zhang,[1] Haifeng Du,[4] Xiaoguang Li,[1, a)] and Yan Zhou[5, b)]
[1)] *College of Engineering Physics, Shenzhen Technology University, Shenzhen, 518118, China*
[2)] *The Center for Advanced Quantum Studies and Department of Physics, Beijing Normal University, 100875 Beijing, China*
[3)] *College of New Materials and New Energies, Shenzhen Technology University, Shenzhen, 518118, China*
[4)] *Anhui Province Key Laboratory of Low-Energy Quantum Materials and Devices, High Magnetic Field Laboratory, HFIPS, Chinese Academy of Sciences, Hefei, 230031, China*
[5)] *School of Science and Engineering, The Chinese University of Hong Kong, Shenzhen, 518172, China*

Magnetic domain wall bimerons (DWBMs) are topological spin textures residing within the magnetic domain walls of in-plane magnets. In this study, we employ both numerical and analytical methods to explore the stabilization of Néel-type DWBMs in a ferromagnet (FM)/heavy metal (HM) bilayer, facilitated by interfacial Dzyaloshinsky-Moriya interaction (DMI), and their dynamics when excited by damping-like spin-orbit torque. Our findings reveal two unique and intriguing dynamic mechanisms, which depend on the polarization direction of the spin current: In the first scenario, the magnetic domain wall serves as a track that confines the motion of the bimeron and effectively suppresses the skyrmion Hall effect. In the second scenario, pushing the magnetic domain wall triggers a rapid sliding of the bimeron along the wall. This process significantly enhances the dynamics of the DWBM, resulting in a velocity increase of approximately 40 times compared to other topological solitons, including skyrmions and bimeron solitons. The damping effect plays a varied role in these mechanisms. Our results highlight the potential advantages of the skyrmion Hall effect in developing energy-efficient spintronic devices based on domain wall bimerons.

A bimeron can be regarded as a counterpart of the skyrmion in in-plane magnets[1–13]. Rooted in the concept of topological solitons, bimerons are essentially composed of two meron entities coupled together to form a compact spin structure. The anisotropic Dzyaloshinsky-Moriya interaction (DMI) plays a key role in the formation of bimeron soliton[3,8]. However, accessible DMI provided by the non-centrosymmetric system or the ferromagnet/heavy interface are both isotropic. In this case, the bimeron solitons are energy-unfavorable, and tend to cluster and form assembly or chain-like structures, which are also reported as domain wall bimeron (DWBM)[14,15]. Recent experimental researches have confirmed the existence of Bloch-type meron chains in the ferromagnetic CoZnMn[16], the ferrimagnetic GdFeCo[17], and the antiferromagnetic CuMnAs[18]. The Néel-type version of DWBM has also been founded in Wan der Waals Ferromagnet FeTeGe[19,20]. Similar to magnetic skyrmions, DWBMs are topologically protected, offering significant thermal stability suitable for long-term storage. The size of a DWBM is generally constrained by the width of the domain wall, which typically spans tens of nanometers in ferromagnets. Moreover, the domain wall can serve as tracks that host DWBMs, showing promise for potential applications in spintronic memory devices. Despite extensive investigations into the stabilization of DWBMs, their dynamics have not yet been reported, and effective methods to manipulate them remain elusive. Notably, the role of the skyrmion Hall effect—an intrinsic characteristic of topological quasi-particles—has not been explored in the dynamics of DWBMs. In this study, we employ both analytical and numerical methods to examine the statics and dynamics of Néel-type DWBM driven by spin-orbit torque. Compared to the bimeron soliton, the thermal stability of DWBM is enhanced by the magnetic domain wall, and it withstands a broad range of DMI strengths. The dynamics excited by the current relate to the polarization direction of the spin current. Our analytical findings suggest that the equivalent force due to magnetic damping is significantly reduced along the domain wall. Consequently, the domain wall can guide the motion of the bimeron and effectively mitigate the skyrmion Hall effect (SHE) [21,22]. More importantly, our results confirm that the spin arrangement of DWBMs allows the skyrmion Hall effect[21,22] to be harnessed as the primary driving force. Therefore, the dynamics of DWBMs can be significantly accelerated, showing an increase in mobility by approximately 40 times compared to several topological solitons, including skyrmions and bimerons, when directly driven by spin-orbit torque (SOT).

Considering a bilayer heterostructure composed of the ferromagnetic thin film hosting DWBM, and the heavy metal layer serving as the spin Hall channel. The free energy of the FM film can be described by

$$E = \int dV \left\{ A_{ex}(\nabla \boldsymbol{m})^2 - K_u(\boldsymbol{m}\cdot\boldsymbol{n})^2 - \frac{1}{2}\mu_0 M_{\mathrm{S}} \boldsymbol{H_d}\cdot\boldsymbol{m} + D_i[m_z\nabla\cdot\boldsymbol{m} - (\boldsymbol{m}\cdot\nabla)m_z] \right\}, \tag{1}$$

[a)] lixiaoguang@sztu.edu.cn
[b)] Zhouyan@cuhk.edu.cn

where the first, second, third, and fourth terms correspond to the energy density of Heisenberg exchange, magnetic anisotropy, dipolar field, and interfacial Dzyaloshinskii-Moriya interaction, respectively. A_{ex}, K_u and D_i are the exchange constant, magnetic anisotropy constant and DMI constant. $\boldsymbol{n} = \boldsymbol{e}_y$ stands for the direction of the anisotropy axis, and $\boldsymbol{H_d}$ is the dipole field.

We employ the Landau-Lifshitz-Gilbert (LLG) equation[23] with the damping-like spin-orbit torque to simulate the dynamics of FM systems, which is described as

$$\frac{\partial \boldsymbol{m}}{\partial t} = -\gamma \boldsymbol{m} \times \boldsymbol{H}_{\text{eff}} + \alpha \boldsymbol{m} \times \frac{\partial \boldsymbol{m}}{\partial t} - \tau_{\text{SH}} \boldsymbol{m} \times (\boldsymbol{m} \times \hat{p}), \quad (2)$$

where $\boldsymbol{m}$ is the normalized magnetization. The damping-like spin-orbit torque $-\tau_{\text{SH}}\boldsymbol{m} \times (\boldsymbol{m} \times \hat{p})$ can be produced by the spin Hall effect of the adjacent HM layer. Here $\hat{p}$ is the polarization vector and the current-dependent coefficient for the damping-like torque is defined as $\tau_{\text{SH}} = \frac{\gamma\hbar}{2\mu_0 e}\frac{j_c\theta_{\text{SH}}}{tM_{\text{S}}}$ with the current density j_c, the reduced Planck constant $\hbar$, the spin Hall angle θ_{SH}, the vacuum permeability constant μ_0, the elementary charge e, and the layer thickness t. γ and α denote the gyromagnetic ratio and the damping constant respectively. $\boldsymbol{H}_{\text{eff}}$ stands for the effective field obtained from the variation of the FM energy in Eq. (1). For subsequent simulations, we utilized the magnetic parameters of CoFeB/Pt[24] , while the DMI constant and damping constant were varied within reasonable range.

Fig. 1 shows the spin structure of the Néel-type DWBM, characterized by a magnetization transition of 360° along the domain wall, and a transition of 180° in the direction normal to it. The magnetic topology of the DWBM is defined by the integer-valued topological charge $Q = \frac{1}{4\pi}\int \mathrm{d}x\mathrm{d}y\ \boldsymbol{m}\cdot(\frac{\partial \boldsymbol{m}}{\partial x} \times \frac{\partial \boldsymbol{m}}{\partial y})$, and the topological charge density is shown in Fig. 1(a). While the distribution of real-space spin and the magnetization components are shown in Fig. 1(b)-(d). We note that the bimeron soliton can be stabilized in the same system. The isotropic DMI breaks the symmetry of its spin structure and introduces nonreprotical dynamics excited by spin current and spin waves[25,26]. We involved this particular excitation in our discussion.

MuMax3[27] is used to perform the micromagnetic simulations. Fig. 2 shows the variation of free energy defined by Eq. (1) as a function of interfacial DMI constant D_i. We use the uniformed magnetization (UM), Néel-type domain wall (DW), bimeron soliton (BMS) and DWBM as the initial states of the simulation, as shown in the inset. Both the energies of DW (green line) and DWBM (red line) decrease with D_i. The critical DMI constant is about 5 mJ/m^2, above which UM becomes energy-unfavorable. Despite an energy penalty over the DW, the DWBM can be stabilized within a wide range of D_i from 1 mJ/m^2 to 6 mJ/m^2. A detailed stabilization phase diagram of DWBM is shown in supplementary material Fig. S1. We note that the Néel-type domain wall plays a role of high energy ground state of DWBM, locally elevates the energy barrier, and subsequently improves its stability. In comparison, the BMS (blue line) exists in a small range of D_i from 4.4 mJ/m^2 to 5.3 mJ/m^2.

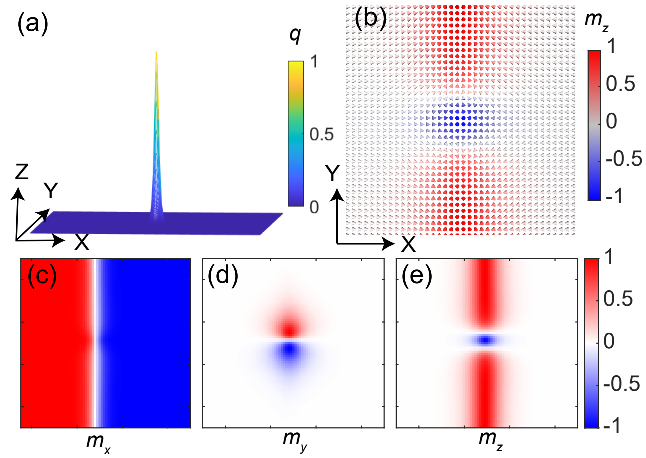

FIG. 1. Spin structure of the DWBM with topological number Q = 1. Distribution of the (a) topological charge density, (b) spin vectors, and (c)-(e) the magnetization components m_x, m_y, and m_z, respectively.

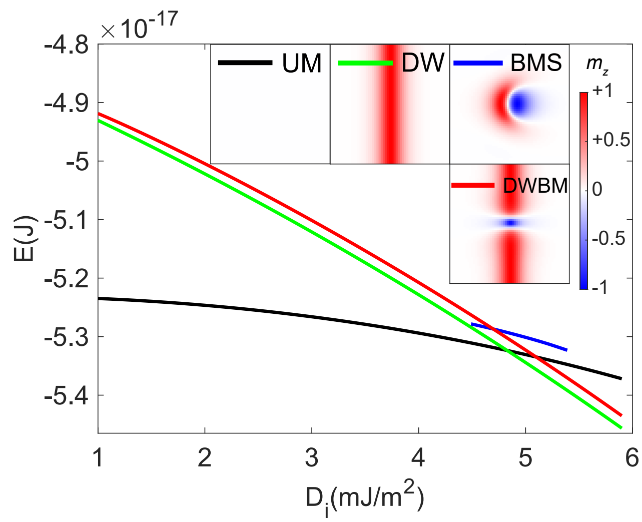

FIG. 2. The total energy of four different magnetic states varies with the Dzyaloshinskii-Moriya interaction constant D_i. The inset shows the initial state used for simulation. In the ensuing simulations, we employ the following parameters: exchange constant A_{ex} = 15 pJ/m, anisotropy coefficient K_u = 0.8 MJ/m^3, DMI strength D_i = 5 mJ/m^2, saturated magnetization M_S = 580 kA/m, gyromagnetic ratio γ = 2.211 $\times 10^5$ m/(A·s) and spin Hall angle θ_{SH} = 0.1. The mesh size of 1024 × 1024 × 1 nm^3 is used. The energy of the system is recorded after the magnetization is fully relaxed.

For the investigation of the DWBM dynamics, we combine numerical and analytical approaches to obtain the motion velocity of DWBM driven by currents with the spin polarization direction in X and Y, respectively. The velocities of DWBM are defined as $v_i = \dot{r}_i$, and the guiding center of the bimeron (r_x, r_y) is numerically calculated by

$$r_i = \frac{\int \mathrm{d}x\mathrm{d}y \left[i\boldsymbol{m} \cdot \left(\frac{\partial \boldsymbol{m}}{\partial x} \times \frac{\partial \boldsymbol{m}}{\partial y} \right) \right]}{\int \mathrm{d}x\mathrm{d}y \left[\boldsymbol{m} \cdot \left(\frac{\partial \boldsymbol{m}}{\partial x} \times \frac{\partial \boldsymbol{m}}{\partial y} \right) \right]}, \quad i = x, y. \tag{3}$$

On the other hand, the dynamics of the DWBM can be analytically expressed by considering the balance between the equivalent forces, which is also known as the Thiele's or the collective coordinate approach[28–31]. We assume the collective motion of both the bimeron and the domain wall, and the steady motion of the spin textures requires

$$\boldsymbol{G} \times \boldsymbol{v} - \alpha \mathcal{D} \boldsymbol{v} - 4\pi \mathcal{C} \hat{p} = \boldsymbol{0}. \tag{4}$$

Here the Magnus force is $\boldsymbol{F}_{\mathrm{G}} = \boldsymbol{G} \times \boldsymbol{v}$ and $\boldsymbol{G} = -4\pi Q \boldsymbol{e}_z$ is the gyrovector. The damping force is $\boldsymbol{F}_\alpha = -\alpha \mathcal{D} \boldsymbol{v}$ and $\mathcal{D} = 4\pi \left[D_{ij} \right]$ represents the dissipative force tensor, in which i, j stands for the coordinate x, y and $D_{ij} = 1/4\pi \int d_{ij}\ \mathrm{d}x\mathrm{d}y$ with the components of the dissipative force density tensor $d_{ij} = \partial_i \boldsymbol{m} \cdot \partial_j \boldsymbol{m}$. The driving force behind the system arises from the damping-like spin-orbit torque, characterized by the expression $\boldsymbol{F}_{\mathrm{SOT}} = -4\pi \mathcal{C} \hat{p}$, where $\mathcal{C}$ represents the driving force tensor defined as $\mathcal{C} = \tau_{\mathrm{SH}} \left[C_{ij} \right]$. And, $C_{ij} = 1/4\pi \int c_{ij}\ \mathrm{d}x\mathrm{d}y$, with the components of the driving force density tensor given by $c_{ij} = (\partial_i \boldsymbol{m} \times \boldsymbol{m})_j$, where the subscript j denotes the jth component of the vector $\partial_i \boldsymbol{m} \times \boldsymbol{m}$. The unit current polarization vector $\hat{p}$ is specified as $\boldsymbol{e}_x$ or $\boldsymbol{e}_y$. Ultimately, Eq. (4) can be reduced to obtain a linear equation for velocity of steady motion in the film plane (Please refer to the Supplementary Material for details),

$$\begin{bmatrix} \alpha D_{xx} & \alpha D_{xy} - Q \\ \alpha D_{yx} + Q & \alpha D_{yy} \end{bmatrix} \begin{bmatrix} v_x \\ v_y \end{bmatrix} = -\tau_{\mathrm{SH}} \begin{bmatrix} C_{xx} & C_{xy} \\ C_{yx} & C_{yy} \end{bmatrix} \begin{bmatrix} p_x \\ p_y \end{bmatrix}. \tag{5}$$

Our initial investigation focused on studying the dynamics of the DWBM driven by spin current polarized in X direction. In this scenario the charge current in the heavy metal layer flows in the direction of the domain wall. Fig. 3(a) shows the schematic diagram of the forces involved. The SOT contributes to a net equivalent force in the +Y direction, which competes the magnetic damping of the DWBM. On the other hand, both the DWBM and the DW contribute to the damping force in -X, resulting in very low mobility in this direction. Considering a system with high damping, the Magnus force of the DWBM could be sufficiently compensated, and thus suppressing the skyrmion Hall effect. Fig. 3(b) shows the corresponding force density distribution when a current with $j_c = 10^{10}\mathrm{A/m^2}$ is applied. Micromagnetic simulation confirms the above mentioned mechanism, as shown in Fig. 4. We observed the linear dependency between the velocity v_x, v_y and the charge current density j_c, as predicted by Eq. (5). Moreover, the translational speed v_x is very small, indicating that the skyrmion Hall effect is effectively mitigated. Since the Néel-type magnetic domian wall is topological trivial, the Magnus force is local, and

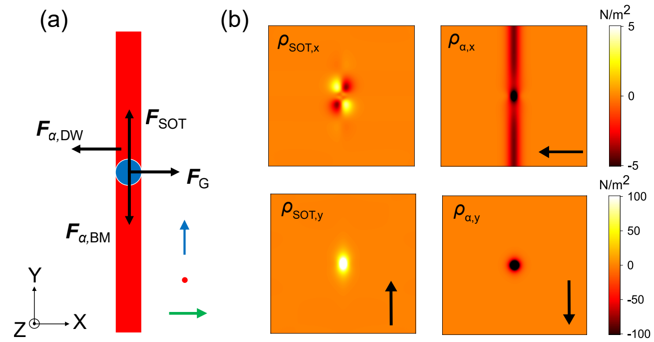

FIG. 3. Dynamic mechanism of DWBM driven by spin current with X polarization. (a) Schematic diagram of the equivalent forces involved, including the damping force of the domain wall $\boldsymbol{F}_{\alpha,\mathrm{DW}}$, and the bimeron $\boldsymbol{F}_{\alpha,\mathrm{BM}}$, the Magnus force $\boldsymbol{F}_G$ and the driving force from SOT $\boldsymbol{F}_{\mathrm{SOT}}$. The red part and the blue part denote the domain wall and the DWBM, respectively. The blue and green arrow in the right corner represent the direction of the DWBM motion and the current polarization, while the red dot indicates the domain wall being static. (b) Distribution of the force density components of SOT, $\rho_{\mathrm{SOT},i}$, and magnetic damping, $\rho_{\alpha,i}$, with the applied current density j_c= $10^{10}\mathrm{A/m^2}$. The black arrows indicating the direction of the resultant force.

tends to bend the magneic domain wall gradually. The bending of the DW is more obvious in the cases with low damping and high current density, leading to the deviation in velocity shown in Fig. 4(a). Fig. 4(b) shows the DWBM velocity as a function of the damping constant α when $j_c = 10^{10}$ A/m^2. The skymion Hall effect observed in the low-damping regime($\alpha < 0.2$) depends on the specific domain wall length used for the analyses. In general, as long as the magnetic domain wall can provide sufficient magnetic damping, the skyrmion Hall effect of the DWBM can be well controlled.

When the charge current is polarized in Y direction, the dynamics of the DWBM is fundamentally different from the above discussed mechanism. Fig. 5(a) shows the schematic diagram of the forces involved in this scenario. The SOT provides the driving forces in -X and +X direction for the DW and the DWBM, respectively. The corresponding force density distribution is shown in Fig. 5(b). Considering the dimension of the DW is much larger than the DWBM, the dynamics of the DW will dominate, and the SOT drives the spin textures into motion in the -X direction. In this case the DWBM is not directly driven by the SOT, but instead follows the collective motion of the DW, leading to a strong Magnus force component in the orthogonal direction (in our case the +Y direction). The Magnus force component competes the magnetic damping of the DWBM, and results in a very high velocity. Briefly, the dynamics of the DWBM is actually boosted by the skyrmion Hall effect. We note this mechanism is entirely different from that of skyrmion or bimeron soliton, for which the Magnus force always joins the magnetic damping force to compete the spin-orbit torque,

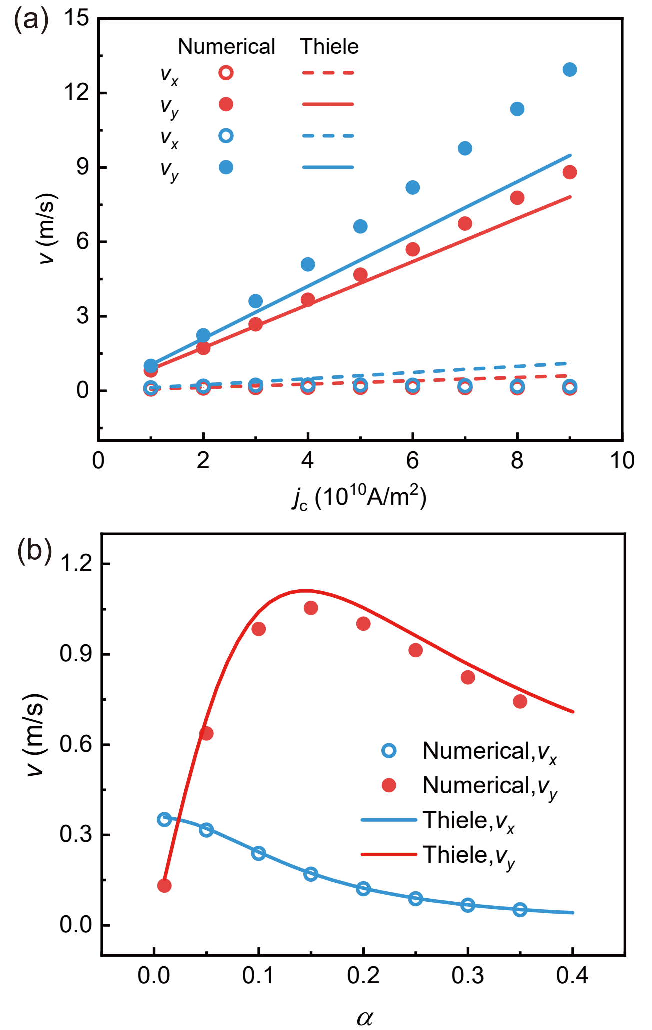

FIG. 4. DWBM velocities introduced by spin current with X polarization. (a) Velocities as functions of current density j_c with damping constant $\alpha = 0.3$ (red) and 0.2 (blue). (b) Velocities as functions of α, with $j_c = 10^{10}\mathrm{A/m^2}$.

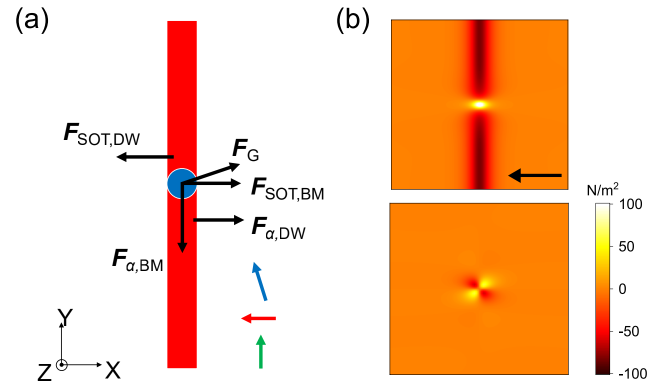

FIG. 5. Dynamic mechanism of DWBM driven by spin current with Y polarization. (a) Schematic diagram of the equivalent forces involved. Noting that the SOT forces for domain wall and DWBM have opposite directions. The blue, red and green arrow in the right corner demonstrate the direction of the DWBM motion, the domain wall motion and the current polarization, respectively. (b) Distribution of the force density components of SOT with the applied current density $j_c = 10^{10}\mathrm{A/m^2}$. The damping force densities remain the same with Fig. 3(b).

and negatively impacts their mobility. Micromagnetic simulations demonstrate the linear relationship between the curren density j_c and the velocity of the DWBM, and we observed a significant improvement in the mobility, which is also confirmed by the analytical results obtained by Eq. (5), as shown in Fig. 6(a). We further compared the speed $|v|$ of the DWBM, bimeron soliton (BMS) and skyrmion (SK) excited by SOT, and the result is shown in Fig. 6(b). The mobility of DWBM is more than an order larger than that of SK or BMS, and non-linearly decreases with α. This is because the magnetic damping force competes with the driving forces from both SOT and skyrmion Hall effect. By decreasing the magnetic damping constant α to 0.05, both numerical simulation and analytical approach confirm a 37 times increase in the mobility of DWBM compared with BMS. Fig. 6(c) visualizes this difference by showing the displacements of DWBMs and the BMS within the same system introduced by spin current (please refer to the Supplementary Video), and Fig. 6(d) shows the corresponding distribution of topological charge density q. Over a period of 6 ns, BMS remains nearly static, while DWBMs with opposite topological number travel fast in the opposite directions, demonstrating the skyrmion Hall effect-based sliding motion. In addition, it is worth-noting that by the direct driving, the SOT force scales with the size of topological spin textures[32,33] , while the Magnus force remains constant due to the conservation of topological charge. For compact spin textures with small size, the dynamics will be dominated by skyrmion Hall effect and the efficiency of spin-orbit torque will significantly decrease. On the other hand, if it is possible to utilize the skyrmion Hall effect as driving force, as here we presented in the scenario of DWBM, higher mobility is achievable. And this will in turn benefit the power consumption of DWBM-based spintronic devices.

In conclusion, we analytically and numerically study the statics of domain wall bimerons, and their dynamics induced by damping-like spin-orbit torque. The numerical simulations show that the domain wall bimeron can be stablized within a wide range of DMI, and the stability is effectively improved compared with the bimeron soliton. The motion of domain wall bimeron induced by spin-orbit torque is also discussed, and speed is analytically derived, which agrees well with the numerical simulations. When the current is applied in the direction of the domian wall, the skyrmion Hall effect of the domain wall bimeron can be effectively suppressed by the damping effect of the magnetic domain wall. More importantly, when the current is applied in the direction perpendic-

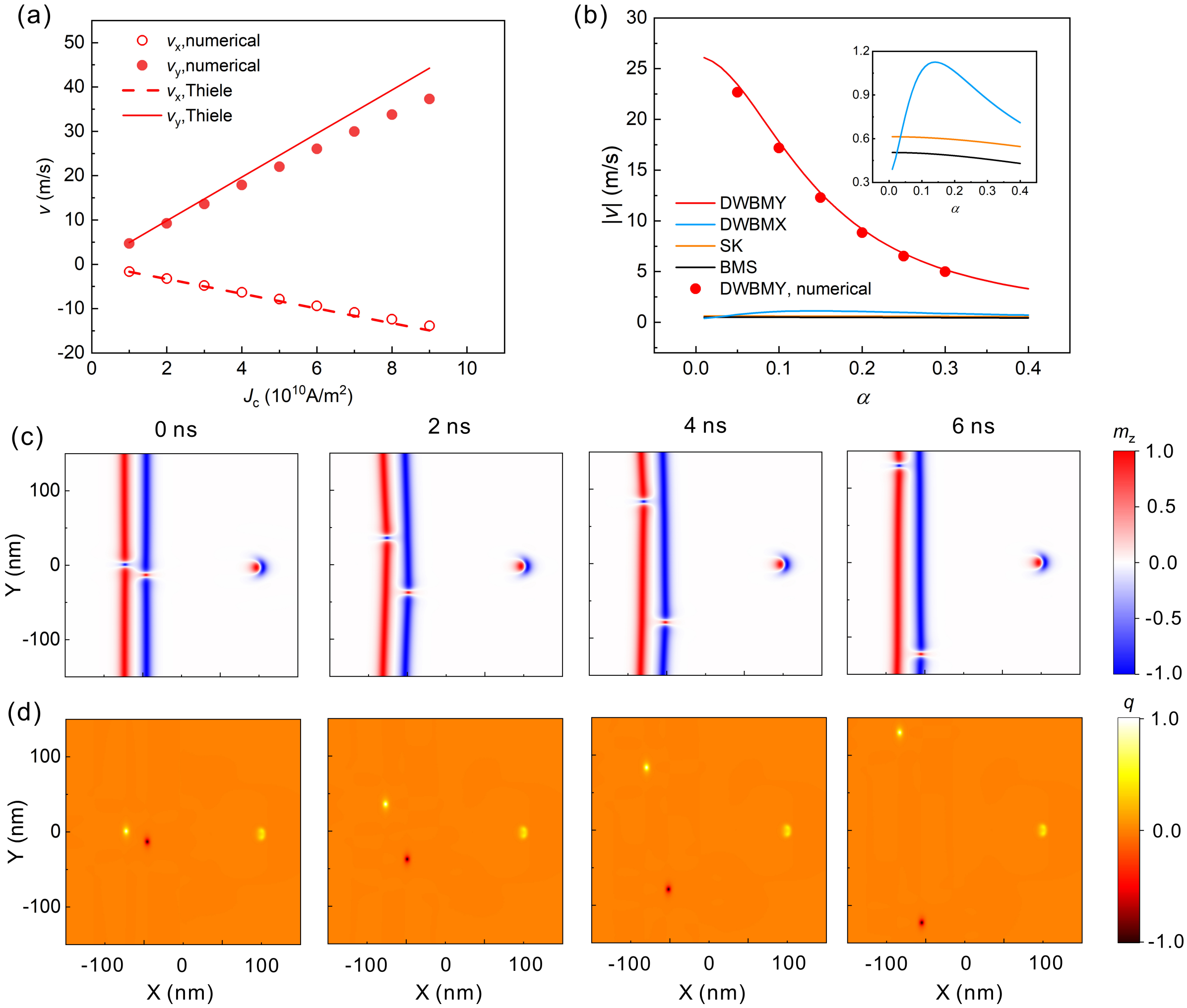

FIG. 6. DWBM velocities introduced by spin current with Y polarization. (a) Velocities as functions of current density j_c with damping constant $\alpha = 0.3$. v_y manifests the skyrmion Hall effect. (b) Speed $|v|$ of DWBM driven by current with X (DWBX) and Y (DWBY) polarization, bimeron soliton (BMS) and skyrmion (SK), as functions of α, with $j_c = 10^{10}\mathrm{A/m^2}$. For the simulation of skyrmion, we used perpendicular magnetic anisotropy and a DMI constant of 3 mJ/m^2, while the other parameters are the same with that of DWBM. Snap shots of (c) magnetization component m_z and (d) topological charge density q when current is applied. The damping constant is set at 0.05.

ular to the domain wall, the skyrmion Hall effect serves as the driving force, and significantly boosts the motion velocity of the domain wall bimeron. Both the numerical simulation and analytical equation demonstrate approximately 40 times increase in the mobility of the domain wall bimeron compared with skyrmion in ferromagnetic films with a damping constant of 0.05. Our results are useful for understanding of the bimeron dynamics and may provide effective ways for building bimeron-based spintronic devices.

Refer to the Supplementary Material for the details regarding linear equation for velocity of steady motion in the film plane and the phase diagram for the size of DWBM. Refer to the Supplementary Video for the sliding motion of the domain wall bimeron introduced by skyrmion Hall effect.

This work was supported by funding from the National Key R&D Program of China (Grant no. 2022YFA1603200, 2022YFA1603202), the National Natural Science Foundation of China (Grant No. 12104322, No. 12375237), the Shenzhen Science and Technology Program (Grant No. ZDSYS20200811143600001), the National Natural Science Foundation of China (Grant No. 52001215), Guangdong Basic and Applied Basic Research Foundation (Grant No. 2021A1515012055), the industrial research and development project of SZTU (Grant No. KY2022QJKCZ005), the Shenzhen Peacock Group Plan (KQTD20180413181702403), the Shenzhen Fundamental Research Fund (Grant No. JCYJ20210324120213037), the Guangdong Basic and Applied Basic Research Foundation (2021B1515120047), the National Natural Science Foundation of China (12374123).

AUTHOR DECLARATIONS

Conflict of Interest

The authors have no conflicts to disclose.

DATA AVAILABILITY

The data that support the findings of this study are available from the corresponding authors upon reasonable request.

REFERENCE

[1] M. Ezawa, Phys. Rev. B **83**, 100408 (2011).
[2] S.-Z. Lin, A. Saxena, and C. D. Batista, Phys. Rev. B **91**, 224407 (2015).
[3] B. Göbel, A. Mook, J. Henk, I. Mertig, and O. A. Tretiakov, Phys. Rev. B **99**, 060407 (2019).
[4] B. Göbel, I. Mertig, and O. A. Tretiakov, Phys. Rep. **895**, 1–28 (2021).
[5] S. K. Kim, Phys. Rev. B **99**, 224406 (2019).
[6] X. Yu, W. Koshibae, Y. Tokunaga, K. Shibata, Y. Taguchi, N. Nagaosa, and Y. Tokura, Nature **564**, 95–98 (2018).
[7] N. Gao, S.-G. Je, M.-Y. Im, J. W. Choi, M. Yang, Q.-c. Li, T. Wang, S. Lee, H.-S. Han, K.-S. Lee, *et al.*, Nat. Commun. **10**, 5603 (2019).
[8] L. Shen, J. Xia, Z. Chen, X. Li, X. Zhang, O. A. Tretiakov, Q. Shao, G. Zhao, X. Liu, M. Ezawa, *et al.*, Phys. Rev. B **105**, 014422 (2022).
[9] K. Ohara, X. Zhang, Y. Chen, S. Kato, J. Xia, M. Ezawa, O. A. Tretiakov, Z. Hou, Y. Zhou, G. Zhao, *et al.*, Nano Lett. **22**, 8559–8566 (2022).
[10] X. Zhang, J. Xia, L. Shen, M. Ezawa, O. A. Tretiakov, G. Zhao, X. Liu, and Y. Zhou, Phys. Rev. B **101**, 144435 (2020).
[11] L. Shen, J. Xia, X. Zhang, M. Ezawa, O. A. Tretiakov, X. Liu, G. Zhao, and Y. Zhou, Phys. Rev. Lett. **124**, 037202 (2020).
[12] F. P. Chmiel, N. Waterfield Price, R. D. Johnson, A. D. Lamirand, J. Schad, G. van der Laan, D. T. Harris, J. Irwin, M. S. Rzchowski, C.-B. Eom, *et al.*, Nat. Mater. **17**, 581–585 (2018).
[13] A. Leonov and I. Kézsmárki, Phys. Rev. B **96**, 014423 (2017).
[14] C. Ross and M. Nitta, Phys. Rev. B **107**, 024422 (2023).
[15] X. Li, L. Shen, Y. Bai, J. Wang, X. Zhang, J. Xia, M. Ezawa, O. A. Tretiakov, X. Xu, M. Mruczkiewicz, *et al.*, npj Comput. Mater. **6**, 169 (2020).
[16] T. Nagase, Y.-G. So, H. Yasui, T. Ishida, H. K. Yoshida, Y. Tanaka, K. Saitoh, N. Ikarashi, Y. Kawaguchi, M. Kuwahara, *et al.*, Nat. Commun. **12**, 3490 (2021).
[17] Z. Li, J. Su, S.-Z. Lin, D. Liu, Y. Gao, S. Wang, H. Wei, T. Zhao, Y. Zhang, J. Cai, *et al.*, Nat. Commun. **12**, 5604 (2021).
[18] O. Amin, S. Poole, S. Reimers, L. Barton, A. Dal Din, F. Maccherozzi, S. Dhesi, V. Novák, F. Krizek, J. Chauhan, *et al.*, Nat. Nanotechnol. **18**, 849–853 (2023).
[19] X. Lv, K. Pei, C. Yang, G. Qin, M. Liu, J. Zhang, and R. Che, ACS Nano **16**, 19319–19327 (2022).
[20] Y. Gao, Q. Yin, Q. Wang, Z. Li, J. Cai, T. Zhao, H. Lei, S. Wang, Y. Zhang, and B. Shen, Advanced Materials **32**, 2005228 (2020).
[21] W. Jiang, P. Upadhyaya, W. Zhang, G. Yu, M. B. Jungfleisch, F. Y. Fradin, J. E. Pearson, Y. Tserkovnyak, K. L. Wang, O. Heinonen, *et al.*, Science **349**, 283–286 (2015).
[22] X. Zhang, Y. Zhou, and M. Ezawa, Nat. Commun. **7**, 10293 (2016).
[23] T. L. Gilbert, IEEE Trans. Magn. **40**, 3443–3449 (2004).
[24] K. Litzius, I. Lemesh, B. Krüger, P. Bassirian, L. Caretta, K. Richter, F. Büttner, K. Sato, O. A. Tretiakov, J. Förster, *et al.*, Nat. Phys. **13**, 170–175 (2017).
[25] X. Liang, J. Lan, G. Zhao, M. Zelent, M. Krawczyk, and Y. Zhou, Physical Review B **108**, 184407 (2023).
[26] L. Shen, X. Li, J. Xia, L. Qiu, X. Zhang, O. A. Tretiakov, M. Ezawa, and Y. Zhou, Phys. Rev. B **102**, 104427 (2020).
[27] A. Vansteenkiste, J. Leliaert, M. Dvornik, M. Helsen, F. Garcia-Sanchez, and B. Van Waeyenberge, AIP advances **4** (2014).
[28] A. Thiele, Phys. Rev. Lett. **30**, 230 (1973).
[29] E. G. Tveten, A. Qaiumzadeh, O. Tretiakov, and A. Brataas, Phys. Rev. Lett. **110**, 127208 (2013).
[30] O. Tretiakov, D. Clarke, G.-W. Chern, Y. B. Bazaliy, and O. Tchernyshyov, Phys. Rev. Lett. **100**, 127204 (2008).
[31] D. Clarke, O. Tretiakov, G.-W. Chern, Y. B. Bazaliy, and O. Tchernyshyov, Phys. Rev. B **78**, 134412 (2008).
[32] L. Shen, X. Li, Y. Zhao, J. Xia, G. Zhao, and Y. Zhou, Phys. Rev. Appl. **12**, 064033 (2019).
[33] S. Rohart and A. Thiaville, Phys. Rev. B **88**, 184422 (2013).